Computer Methods in Applied Mechanics and Engineering 89 (1991) 309–336
North-Holland

The COC algorithm, Part II: Topological, geometrical and generalized shape optimization

M. Zhou and G.I.N. Rozvany
FB 10, Essen University, W-4300 Essen 1, Germany

Received 15 November 1990
Revised manuscript received 1 February 1991

After outlining analytical methods for layout optimization and illustrating them with examples, the COC algorithm is applied to the simultaneous optimization of the topology and geometry of trusses with many thousand potential members. The numerical results obtained are shown to be in close agreement (up to twelve significant digits) with analytical results. Finally, the problem of generalized shape optimization (finding the best boundary topology and shape) is discussed.

1. Introduction

General aspects of the COC algorithm and its applications to cross-section optimization were discussed in Part I of this study [1]. Simultaneous optimization of the topology and geometry by means of COC methods, as well as generalized shape optimization are discussed in this paper.

Layout optimization consists of three simultaneous operations, namely
(a) topological optimization (spatial sequence or configuration of members and joints),
(b) geometrical optimization (location of joints and shape of member axes), and
(c) optimization of the cross-sections.

One of the difficulties in shape optimization is that the optimal shape may represent a multiply connected set with internal boundaries whose topology is not known and is difficult to determine, because new internal boundaries cannot be easily generated. Moreover, in many optimization problems the theoretical optimal shape contains an infinite number of internal boundaries. The determination of the topology then becomes a layout optimization problem.

Generalized shape optimization is aimed at determining simultaneously the boundary topology and boundary shape. The optimal solution of these problems contains three types of regions, namely (a) solid (black), (b) empty (white) and (c) perforated (grey) regions.

Geometrically unconstrained cross-section (thickness) optimization of plates and shells often results in a, theoretically, infinite number of rib-like formations whose layout must be optimized. This means that both cross-section and shape optimization may require, in effect, layout optimization.

Layout optimization is the most complex task in structural optimization because
– one has a choice of an infinite number of possible topologies, and

– for each point of the structural domain, there exist an infinite number of member directions. The cross-section of non-vanishing (optimal) members must be optimized simultaneously.

Layout optimization is important because it enables much greater material savings than pure cross-section optimization.

To illustrate this point on a simple example, we consider the problem in Fig. 1(a), in which four point loads P are required to be transmitted by beams of constant depth to simple supports along the boundary of a square domain. In the first solution shown (Fig. 1(b)), the total 'moment area' (area of the moment diagrams), which is a measure of structural weight, is $6Pa^2$. The optimal beam layout in Fig. 1(c) gives a total moment area of $4Pa^2$. The weight difference of 50% is much greater than the usual savings achieved by cross-section optimization.

An even bigger difference between the weight of optimal and nonoptimal layouts is found for the boundary and loading condition in Fig. 2(a), in which the transverse point load P is to be transmitted to two simply supported edges (double lines) of a rectangular domain. The other two edges are unsupported. Figure 2(b) shows the optimal beam layout and the corresponding moment diagrams with a total moment area of $8Pa^2$. The nonoptimal layout shown in Fig. 2(c) has a moment area of $17Pa^2$ which exceeds the optimal one by 112.5%. It has been shown [2] that for long span grillages, for which the selfweight is a significant load condition, this difference between optimal and nonoptimal structural weights is often over 1000%.

The most systematic analytical method for layout optimization is the so-called layout theory, developed by Prager and Rozvany in the late seventies and extended by the research teams of the latter in the eighties. This theory is a generalization of an approach used around the turn of the century by Michell [3] (see Part I, Section 2.2), who made use of some ideas by Maxwell [4]. Layout theory is based on two underlying concepts, namely,

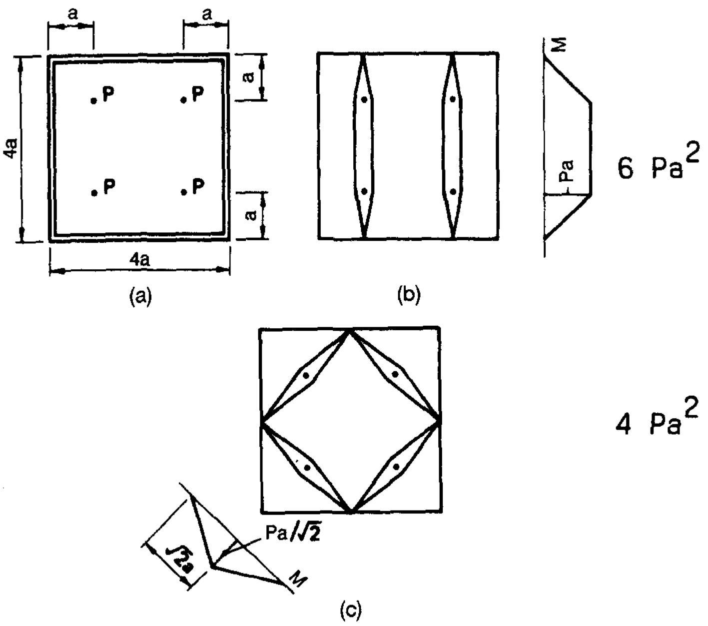

Fig. 1. Comparison of optimal and non-optimal beam layouts.

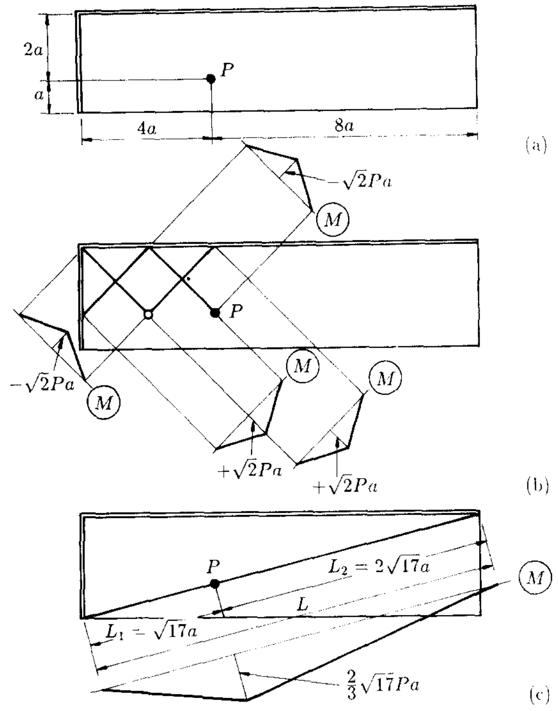

Fig. 2. Another comparison of optimal and non-optimal beam layouts.

(a) the structural universe, which is the union of all feasible or potential members, and
(b) continuum-based or static-kinematic optimality criteria, which are mathematical conditions for the optimality of a structure, reinterpreted in terms of a fictitious adjoint structure (see Sections 2–5 of Part I).

The adjoint strain–stress relations give a strain requirement, usually in the form of an inequality, also along vanishing members (having a zero cross-sectional area and zero generalized stress). This means that in convex problems, for which the optimality criteria represent sufficient conditions, their fulfilment for the entire structural universe also represents a sufficient condition of optimality for the structural layout.

As was explained lucidly by Kirsch [5], layout optimization problems are solved by the numerical school in two stages. First, topological optimization is carried out by assuming a 'highly connected' ground structure (in this paper: structural universe) and then removing non-optimal members. The second stage consists of geometrical optimization, in which the topology is assumed to be fixed (unless some joints coalesce during the solution process) and the design variables are the coordinates of the joints and the cross-sectional areas. The above design variables are usually optimized by mathematical programming methods.

Topological optimization in the past, even with simplifying assumptions and approximations, was restricted to a small number of potential members because of the limited optimization capability of the mathematical programming methods used. Kirsch [5], for example, uses only 8 potential members in one half of a symmetric truss. Due to the introduction of iterative COC methods, to be described in Section 3, it has become possible to investigate structural universes with many thousand potential members.

Earlier formulations of the layout theory for structural design were introduced by Prager and Rozvany [6–8], and more up-to-date reviews of this field were offered in principal lectures of NATO ASI's [9–11], in a book chapter [12] and, in particular, in a recent book [2] by the latter.

2. Analytical methods for layout optimization

The general ideas of layout theory will be explained through examples involving the following two types of structures:
- beams having rectangular cross-sections of given depth and variable width, and
- trusses or pin-jointed frames.

The two types of design conditions to be considered here will be
- optimal plastic design for a given ultimate load, and
- optimal elastic design for a given compliance (the sum of products of external forces and the corresponding deflections).

2.1. Optimal plastic design

The fundamental relations for this class of problems were given in Fig. 2 of Part I [1]. We restrict our treatment to a specific cost function of the form

$$\psi = k|Q|\,, \qquad \Phi = \int_D k|Q|\,\mathrm{d}x\,, \tag{1}$$

where k is a given constant, ψ the member weight per unit length, Q is the relevant generalized stress, Φ is the total structural weight and D is the structural domain. For trusses we have $Q = N$ (where N is the axial member force) and $k = \gamma/\sigma_0$ (where γ is the specific weight of the truss material and $\pm\sigma_0$ is the yield stress in tension and compression). For beams of variable width z, but given depth h, we have $Q = M$ (where M is the bending moment) and $k = 4\gamma/h\sigma_0$ (see also Section 2.3 of Part I).

Before evaluating the optimality conditions for the above class of problems, we clarify once more that the generalized gradient $\mathscr{G}$ for a cost function of one variable $\psi(Q)$ has the meaning

$$\mathscr{G}(\psi) = \mathrm{d}\psi/\mathrm{d}Q\,, \tag{2}$$

if $\psi(Q)$ is differentiable at the considered Q-value, and it becomes

$$\mathscr{G}(\psi) = \nu(\mathrm{d}\psi/\mathrm{d}Q)^- + (1-\nu)(\mathrm{d}\psi/\mathrm{d}Q)^+\,, \quad 0 \le \nu \le 1\,, \tag{3}$$

if $\psi(Q)$ has a cusp at the considered Q-value, where $(\mathrm{d}\psi/\mathrm{d}Q)^-$ and $(\mathrm{d}\psi/\mathrm{d}Q)^+$ represent the slope to the left and right of the cusp. Then it follows from Fig. 2 or (6) in Part I [1] that the adjoint strain for the specific cost function in (1) becomes

$$\bar{q} = k \operatorname{sgn} Q \quad \text{for } Q \neq 0\,, \tag{4}$$

$$|\bar{q}| \leq k \quad \text{for } Q = 0\,, \tag{5}$$

in which $\bar{q} = \bar{\varepsilon}$ (where $\bar{\varepsilon}$ is the adjoint axial strain) for trusses and $\bar{q} = \bar{\kappa}$ (where $\bar{\kappa}$ is the curvature) for beams.

These optimality conditions were represented graphically, in the context of beams, in Fig. 3(c) of Part I.

2.2. Optimal elastic design for a given compliance

In the literature, 'compliance' means the product of the external loads and the corresponding displacements

$$C = \int_D \boldsymbol{p} \cdot \boldsymbol{u}\, \mathrm{d}\boldsymbol{x}\,. \tag{6}$$

In the case of a compliance constraint, the virtual load becomes identical with the real load $\bar{\boldsymbol{p}} = \boldsymbol{p}$ and hence in Fig. 5 of Part I [1] the real and adjoint systems are also the same, with $\bar{\boldsymbol{Q}} = \boldsymbol{Q}$ and $\bar{\boldsymbol{q}} = \boldsymbol{q}$.

We consider the class of problems with single-component generalized stress and strain

$$\boldsymbol{Q} = Q\,, \qquad \boldsymbol{q} = q\,, \qquad \psi = cz\,, \qquad [\boldsymbol{F}] = 1/rz\,, \tag{7}$$

where c and r are given constants and z is a cross-sectional variable. Then the optimality criterion in (23) of Part I is replaced by

$$z = \sqrt{\nu/rc}\,|Q|\,. \tag{8}$$

If a minimum value for z is prescribed ($z \geq z_a$), then we have [cf. (34) in Part I]

$$(\text{for } \sqrt{\nu/rc}\,|Q| > z_a) \quad z = \sqrt{\nu/rc}\,|Q|\,, \tag{9}$$

$$(\text{for } \sqrt{\nu/rc}\,|Q| \leq z_a) \quad z = z_a\,. \tag{10}$$

Since in this class of problems $\bar{q} = \bar{Q}/rz = Q/rz$, (7) and (9) imply

$$(\text{for } \sqrt{\nu/rc}\,|Q| > z_a,\, z > z_a) \quad \bar{q} = Q/rz = \sqrt{c/r\nu}\,\operatorname{sgn}|Q|\,, \tag{11}$$

$$(\text{for } \sqrt{\nu/rc}\,|Q| \leq z_a,\, z = z_a) \quad |\bar{q}| = |Q|/(rz_a) \leq \sqrt{c/r\nu}\,. \tag{12}$$

After a limiting process with $z_a \to 0$ and replacing $\sqrt{c/r\nu}$ with k, we can see that (11) and (12) reduce to (4) and (5). This means that, within a constant factor, the optimality criteria for optimal plastic design and optimal elastic design for compliance are identical for both trusses and beams of given depth. This confirms earlier observations regarding Michell frames by Hegemier and Prager [13]. These authors have also shown that the same solutions (within a constant factor) are valid for given natural frequency and for given stiffness in stationary creep.

The value of the multiplier ν can be determined from the work equation and (8) as

$$C = \int_D pu \, \mathrm{d}x = \int_D \frac{Q^2}{rz} \, \mathrm{d}x = \int_D \frac{Q^2}{r\sqrt{\nu/rc}\,|Q|} \, \mathrm{d}x = \int_D \frac{|Q|}{\sqrt{\nu r/c}} \, \mathrm{d}x \,, \tag{13}$$

furnishing

$$\sqrt{\nu} = \int_D |Q| \, \mathrm{d}x / (C\sqrt{r/c}) \,. \tag{14}$$

Moreover, for the total cost (weight) Φ we have by (7), (9) and (14) for $z_a \to 0$

$$\Phi = \int_D cz \, \mathrm{d}x = \int_D c\sqrt{\nu/rc}\,|Q| \, \mathrm{d}x = \frac{c}{r}\left(\int_D |Q| \, \mathrm{d}x\right)^2 / C \,. \tag{15}$$

2.3. Elementary examples illustrating applications of the layout theory

2.3.1. Two-span beam with a central point load over one span

This is a very simple layout problem in which the structural universe consists of two beam spans. Over one of the spans the beam cross-section may take on a zero area. Since the optimal deflection diagrams can be subjected to a linear transformation, the constant k in (4) and (5) or $\sqrt{\nu/cr}$ in (11) and (12) with $z_a = 0$ will be replaced by unity and then for $Q = M$ and $\bar{q} = \bar{\kappa}$ the normalized adjoint beam curvatures for both plastic and elastic design are

$$(\text{for } |M| > 0) \quad \bar{\kappa} = \operatorname{sgn} M \,, \tag{16}$$

$$(\text{for } |M| = 0) \quad |\bar{\kappa}| \leqslant 1 \,. \tag{17}$$

Moreover, the optimal values of the width in elastic compliance design are given by (9) as

$$z = \sqrt{\nu/cr}\,|M| \,. \tag{18}$$

It will be shown that the solution depends on the ratio of the loaded and unloaded spans. In Fig. 3(a), this ratio is 1:2. Assuming that the beam takes on a zero cross-sectional area over the longer span, we have the moment diagram in Fig. 3(c) and the adjoint deflection diagram in Fig. 3(b) satisfies the curvature conditions in (16) and (17). Note that for the vanishing beam region over the longer span we still have an adjoint deflection[1] diagram which plays an important role in determining the optimal solution. By (18) the diagram in Fig. 3(c) also represents the variation of $z/\sqrt{\nu/rc}$. Prescribing a compliance value of $C = 1$ (corresponding to a unit deflection at the loaded point), the moment area A in Fig. 3(c) and (15) with $C = 1$, $Q \to M$ furnish the beam weight

$$\Phi = (1/8)^2 = 1/64 = 0.015625 \,. \tag{19}$$

[1] In Fig. 3, the normalized values of the real and adjoint deflections are the same for non-vanishing cross-sections and hence κ refers to both real and adjoint curvatures.

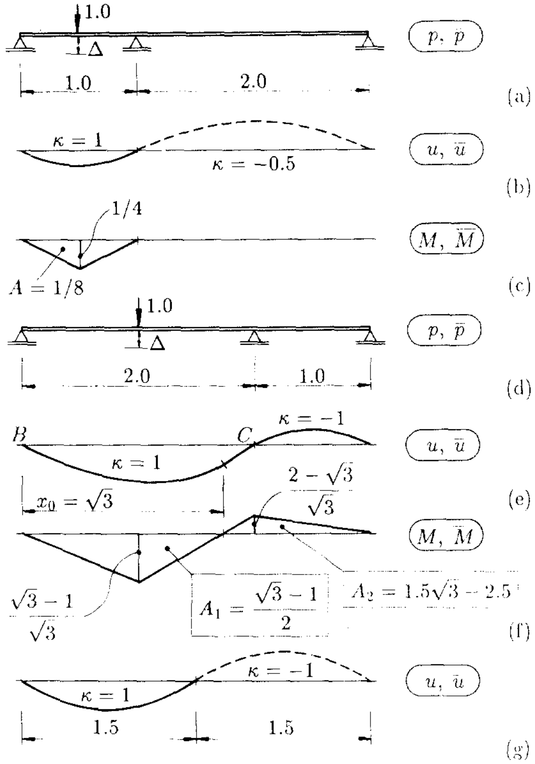

Fig. 3. A simple layout problem: two-span beam.

If we now change the ratio of the loaded and unloaded spans to 2:1 (Fig. 3(d)), then the type of moment diagrams in Fig. 3(f) would require by (16) the adjoint deflection diagram in Fig. 3(e). In the latter, the slope at the support C is $\mathrm{d}u/\mathrm{d}x = 0.5$ and then the end condition $u_B = 0$ requires $2(0.5) + (2 - x_0)(2 + x_0)/2 - x_0^2/2 = 0$, giving $x_0 = \sqrt{3}$. The moment diagram in Fig. 3(f), whose absolute value also represents $z/\sqrt{\nu/rc}$, can then be determined from simple statical considerations. By (15), the normalized beam weight becomes

$$(A_1 + A_2)^2 = (2\sqrt{3} - 3)^2 = 0.215390309\,. \tag{20}$$

The above solutions will be verified by numerical (iterative COC) calculations in Section 3.2.1.

It is still interesting to know, at which span ratio the elementary topology in Figs. 3(a–c) changes to the topology in Figs. 3(d–f).

Clearly, the topology represented by Figs. 3(a–c) is valid up to a span ratio of 1:1, at which the curvature in the unloaded span also reaches $\kappa = 1$. Beyond this span ratio, the condition in (17) does not allow a zero cross-sectional area in the unloaded span.

Note that all moment diagrams in this section had to be statically admissible and the corresponding adjoint curvatures kinematically admissible in order to fulfill the optimality condition in Fig. 5 in Section 3.3 of Part I [1].

2.3.2. Least-weight pin-jointed frame for a point load parallel to a supporting line

In the case of pin-jointed frames, the generalized stress is the axial force $\boldsymbol{Q} = N$ and the generalized strain is the axial member strain $\boldsymbol{q} = \varepsilon$. Then the general optimality conditions (4) and (5) for optimal plastic design reduce to Michell's optimality criteria [(1) and (2) in Part I] and for optimal elastic design with given compliance, (11) and (12) with $z_a = 0$ give the same solution within a constant multiplier. In this, and the next two examples, therefore, we shall consider plastic design for simplicity. The relevant optimality criteria are repeated here in a normalized form (with $k = 1$) for convenience

$$(\text{for } |N| > 0) \quad \varepsilon = \operatorname{sgn} N \,, \tag{21}$$

$$(\text{for } |N| = 0) \quad |\varepsilon| \leqslant 1 \,. \tag{22}$$

Figure 4(a) shows the loading and a structural universe for the considered problem and Fig. 4(b) the optimal solution which can be proved as follows. One must find a displacement field satisfying (21) and (22), as well as the kinematic boundary conditions, that is, zero displacements in all directions along the vertical support. This means that along the two bars in Fig. 4(b) the strains must be $\varepsilon = 1$ and $\varepsilon = -1$, respectively, and along all other members in Fig. 4(a) the absolute value of ε must not exceed unity. Denoting the displacements in the x and y directions in Fig. 4(b) by u and v, a displacement field satisfying the above conditions is

$$u(x, y) \equiv 0 \,, \quad v(x, y) = -2x \,, \tag{23}$$

which clearly satisfies the kinematic boundary conditions $u_x \equiv u_y \equiv 0$ along the support with $x = 0$. Moreover, the strains in the x and y directions are

$$\varepsilon_x = \frac{\partial u}{\partial x} = 0 \,, \qquad \varepsilon_y = \frac{\partial v}{\partial y} = 0 \,, \qquad \gamma_{xy} = \frac{\partial u}{\partial y} + \frac{\partial v}{\partial x} = -2 \,. \tag{24}$$

Then in the principal directions at 45° to the vertical, the principal strain values become

$$\varepsilon_1 = 1 \,, \qquad \varepsilon_2 = -1 \,. \tag{25}$$

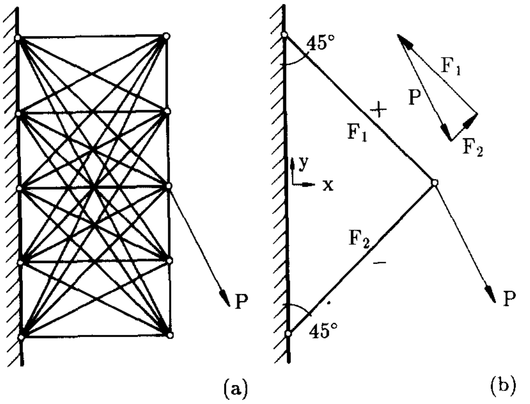

Fig. 4. Optimal layout of a simple pin-jointed frame.

The above displacement field, therefore, satisfies (21) along the non-vanishing members in Fig. 4(a), in which the forces are statically admissible. Moreover, since the principal strains represent the directionally highest absolute values of the strains, (22) is also fulfilled for any vanishing member in Fig. 4(a). In fact, the same solution would be still valid, if the structural universe consisted of all possible members contained in the half-plane to the right of the vertical support in Fig. 4(a).

2.3.3. Optimal transmission of a vertical point load to supports formed by a horizontal and a vertical line

It can be shown that in the above problem, the optimal topology depends on the ratio of the distances of the vertical point load from the vertical and horizontal supporting lines. The analytical proof is based on the adjoint field given in Fig. 5(b), in which the displacements satisfy all kinematic boundary conditions, as well as continuity conditions along the boundary of the two regions indicated. Arrow-like symbols indicate the direction and sign of principal strains having a unit value, along which, by optimality condition (21), a non-zero force is admitted. This means that for loads above the region boundary with a slope 2:1, the optimal topology consists of two bars of 45° to the vertical and for loads below that boundary the optimal topology consists of a single vertical bar. Examples of the optimal load transmission are given in Fig. 5(a).

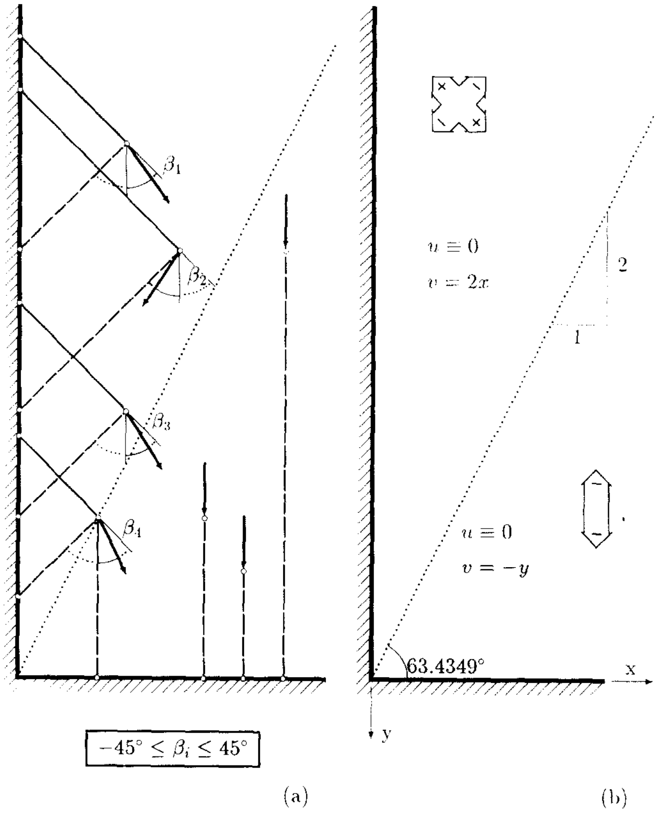

Fig. 5. Adjoint field (b) and optimal layout (a) for a corner region with a point load.

2.4. Analytical solutions for least-weight grillages (beam systems), trusses and shell-grids

The above layout theory was particularly successful in providing analytical solutions for least-weight grillages considering almost all possible boundary and loading conditions [2, 6–12], as well as for shell-grids (arch-grids) [9–12]. More recently, a systematic survey of least-weight trusses for various boundary conditions was carried out [14, 20].

3. Layout optimization using the iterative COC algorithm

3.1. General formulation

For the layout of all elastic systems with a deflection constraint, basically the same procedure can be adopted as the one described in Section 3.6 of Part I [1]. The main difference is that, for the prescribed minimum value z_{ia} of the parameter z_i, the smallest possible value (e.g. 10^{-12} times the average value of that parameter) is used which can still be handled by a program with double precision and does not cause ill-conditioning.

3.2. Elementary examples of layout optimization by the iterative COC method

3.2.1. Two-span beams with a central unit point load over one span

The problem solved analytically in Section 2.3.1 was also computed by the iterative COC procedure using a prescribed minimum width value of $z_{ia} = 10^{-8}$ with $N = 300$ and $N = 1800$ elements. For the span ratio in Fig. 3(a), the COC method yielded total cost values of $\Phi_{300} = 0.015625018$ (22 iterations) and $\Phi_{1800} = 0.015625013$ (21 iterations), both showing a 7-digit agreement with the analytical result in (19). For the span ratio in Fig. 3(d), the COC procedure yielded $\Phi_{300} = 0.21540290$ (22 iterations) and $\Phi_{1800} = 0.21539237$ (36 iterations), which represents four and five digits agreements, respectively, with the analytical result in (20). The above iteration numbers were required for a convergence tolerance value of $\bar{E} = 10^{-6}$ [see (35) in Part I], but a Φ-value with an error of less than 2% was obtained already after 3 iterations. The convergence was near-uniform, both the Φ-values and their differences decreasing monotonically.

3.2.2. Simple pin-jointed frames

Figures 6(a–c) show some simple truss layout problems which were solved for given compliance by the iterative COC method. Members indicated in thick lines represent optimal bars in analytical solutions (see, for example, Fig. 5). Figure 6(d) shows the convergence history for the truss in Fig. 6(b). The 'weight' $\tilde{\Phi}$ here is nondimensional, $\tilde{\Phi} = \Phi E\Delta/(PL^2\gamma)$, where Φ is the total weight of the structure, E is Young's modulus, Δ is the prescribed deflection, P is the point load, L is the dimension shown in Fig. 6 and γ is the specific weight of the material used. The 'scaled weight' $\tilde{\Phi}_s$ corresponds to a truss in which all cross-sections are linearly scaled to satisfy the compliance (deflection) condition exactly.

For these problems, the COC method was combined with either (a) a finite element (FE) program developed by the first author, or (b) ANSYS. Both FE programs yielded identical results.

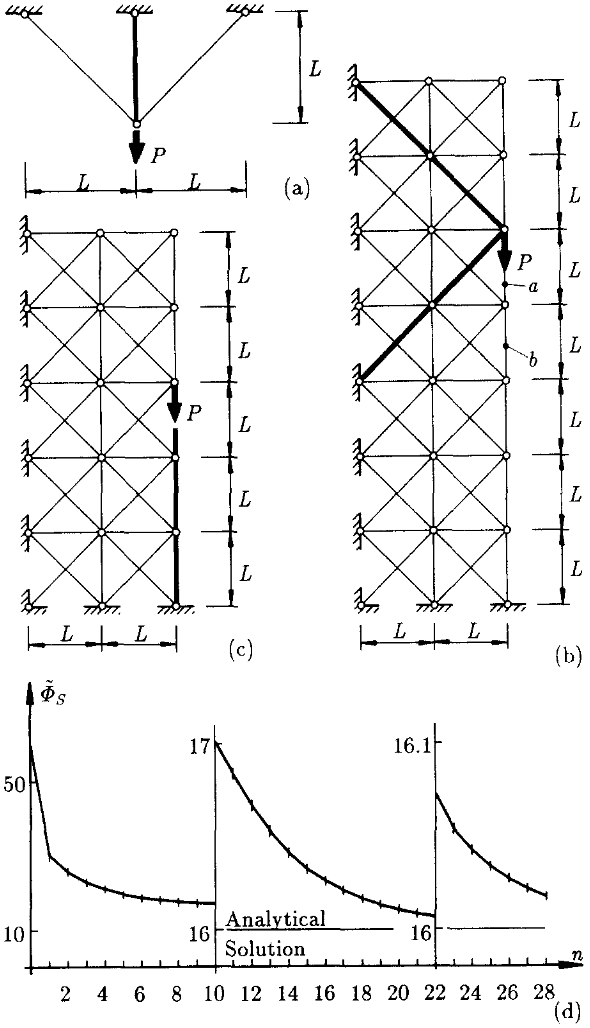

Fig. 6. (a)–(c) Various simple layout optimization problems solved by iterative COC methods. (d) Non-dimensional scaled structural weight $\tilde{\Phi}_s$ versus number of iterations n for the problem under (b).

Using the nondimensionalization given above for $\tilde{\Phi}$, the exact optimal weight for the 56-bar truss (Fig. 6(b)) is $\tilde{\Phi} = 16$ and the iterative COC procedure yielded after 126 iterations a weight of $\tilde{\Phi}_S = 16.000000000048$, which represents an agreement of twelve significant digits. In the COC solution, all non-optimal members took on the prescribed minimum cross-section ($\tilde{z}_a = 10^{-12}$), except members a and b (Fig. 6(b)) which had a cross-sectional area of $\tilde{z}_i = 2.88 \cdot 10^{-12}$ and $\tilde{z}_i = 1.74 \cdot 10^{-12}$. This indicates that all non-optimal members vanish when $\tilde{z}_a \to 0$, as in the analytical solution. The cross-sections of the optimal members agreed with the analytical solution for the first 12 significant digits.

In the 40-bar problem (Fig. 6(c)), *all* non-optimal members took on the value of $\tilde{z}_a = 10^{-12}$ in the iterative COC solution and the cross-sectional area for the optimal members agreed again with the analytical solution.

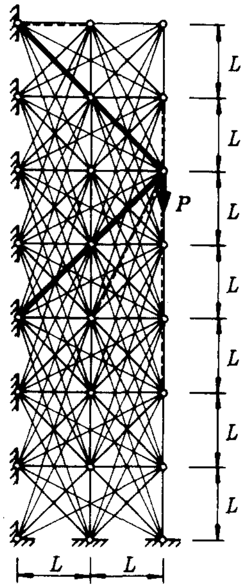

Fig. 7. A more complex structural universe with 114 members for the example in Fig. 6(b).

The problem in Fig. 6(b) (56-bar truss) was also run on the COC program with a structural universe having 114 members (Fig. 7). The optimal members (thick lines) again took on a cross-sectional area of 2.8284271 ($\approx 2\sqrt{2}$) and all other members took on the prescribed minimum value of 10^{-12}, except the ones marked with a broken line, which were all under 10^{-11}. The above run yielded an optimal total cost value of 16.00000000016 after 231 iterations. The larger error compared to the analytical solution is due to the larger number and the greater average length of the members with the minimum cross-section.

The same problem was also investigated with a structural universe having 804 members (Fig. 8(a)). The optimal members are again shown in thick line (Fig. 8(b)) and the members having an area slightly greater than the prescribed minimum value ($10^{-12} < z_i < 10^{-11}$) in broken line. The unusually stringent convergence criterion of $(\Phi_{\text{new}} - \Phi_{\text{old}})/\Phi_{\text{new}} < 10^{-14}$ was satisfied after 627 iterations and gave a total cost value of 16.00000000081.

At the time of these investigations, the analytical solution was not available. It was obtained somewhat later [14] and is given in Fig. 5 herein.

4. More advanced examples of layout optimization by the iterative COC method

4.1. Truss-like continuum containing a Hencky net

It was pointed out by Prager (e.g. [6]) that many least-weight truss layouts consist of an infinite number of members having an infinitesimal spacing and hence they should be termed 'truss-like continua'. One such optimal layout is shown in Fig. 9(a) in which the truss is restricted to the rectangle *ABCD* and a point load $P = 1$ is to be transmitted to the shorter side at the opposite end. The triangle *ACE* contains no members on its interior and the

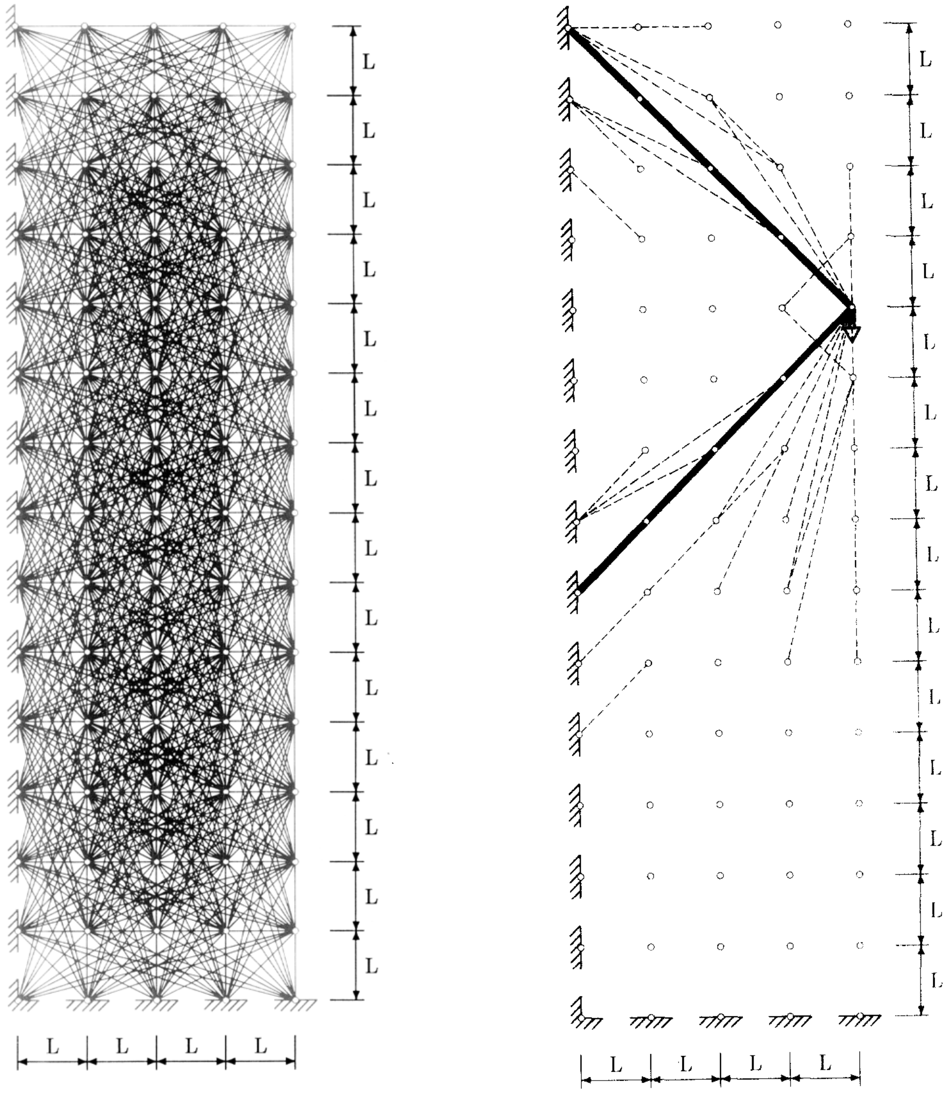

Fig. 8. (a) Structural universe with 804 members for the problem in Fig. 6(b). (b) COC results.

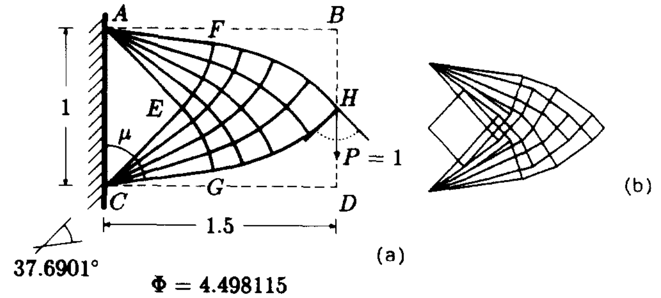

Fig. 9. Optimal layout consisting partly of a Henky net: (a) analytical, (b) COC solution.

regions AEF and CEG consist of straight radial members. The region $EFGH$ is a Hencky net with curved members. For obvious reasons, only a finite number of members are indicated. The analytical solution of the above problem is discussed by Hemp ([15, pp. 97–99]). For a side ratio of 1.5 to 1.0, Hemp's equation (4.120) gives

$$1.5 = \frac{1}{2}\int_0^{2\mu}[I_0(t) + I_1(t)]\,dt = \frac{1}{2}\left[I_0(2\mu) - 1 + 2\sum_{n=0}^{\infty}(-1)^n I_{2n+1}(2\mu)\right], \tag{26}$$

yielding the angle $\mu = 82.690133°$. Then the total truss volume can be calculated from Hemp's equations (4.123) for a unit load and $k = 1$ (in Hemp's notation $\sqrt{2}FR/\sigma = 1$) as

$$\Phi = (1 + 2\mu)I_0(2\mu) + 2\mu I_1(2\mu), \tag{27}$$

where I_0 and I_1 are modified Bessel functions. For the above μ-value, (26) gives the optimal truss volume

$$\Phi_{\text{opt,plastic}} = 4.498115. \tag{28}$$

The above value represents an optimal plastic design [(1) with $k = 1$]. For elastic design with a compliance constraint ($C = 1$) we have by (15) with $c = r = 1$

$$\Phi_{\text{opt,compliance}} = 4.498115^2 = 20.233042. \tag{29}$$

Using the iterative COC algorithm and structural universes with 5055 and 12992 members, respectively, truss volumes of $\Phi = 20.540807$ and $\Phi = 20.419699$ were obtained for elastic design with a compliance constraint. For plastic design, by (1) with $k = 1$ and (15) with $C = 1$, the square root of the above values must be taken, giving $\Phi = 4.532197$ and $\Phi = 4.518816$, which represent 0.76% and 0.46% errors compared to the analytical solution. In the above procedure, a minimum prescribed cross-sectional area of 10^{-12} was used. The system with 5055 members required over 3500 iterations with a convergence tolerance value of $\bar{E} = 10^{-8}$ [see (35) in Section 3.6 of Part I [1]], but a Φ-value of 20.77 was reached already after 100 iterations (1% error compared to the value after satisfaction of the convergence criterion). The layout of members having a cross-sectional area over $z = 0.1$ in elastic compliance design is shown in Fig. 9(b), which exhibits clear similarities with the analytical solution in Fig. 9(a).

The above cross-sectional area [by (1) with $k = 1$, as well as (8) and (14) with $c = r = C = 1$] corresponds to $z = 0.1/\Phi_{\text{opt,plastic}} = 0.1/4.498115 \approx 0.0222$ in plastic design.

4.2. Single point load parallel to a supporting line, triangular structural domain

For the above problem, in which the structural members are restricted to the triangle ABC in Fig. 10, with a support along AB and free edges along AC and BC, the fairly obvious analytical solution consists of members running along the free edges of the domain (Fig. 10). Before a rather complicated proof for the above solution was found [20], the same problem was investigated by the iterative COC procedure, using a structural universe with 720 members (Fig. 11). The analytical solution for the above problem yields $\Phi = 25$ and the

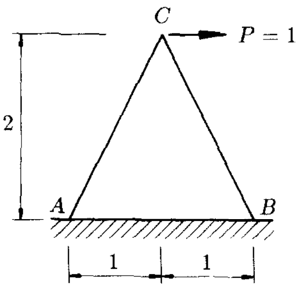

Fig. 10. Loading and analytical solution for a layout restricted to a triangular domain.

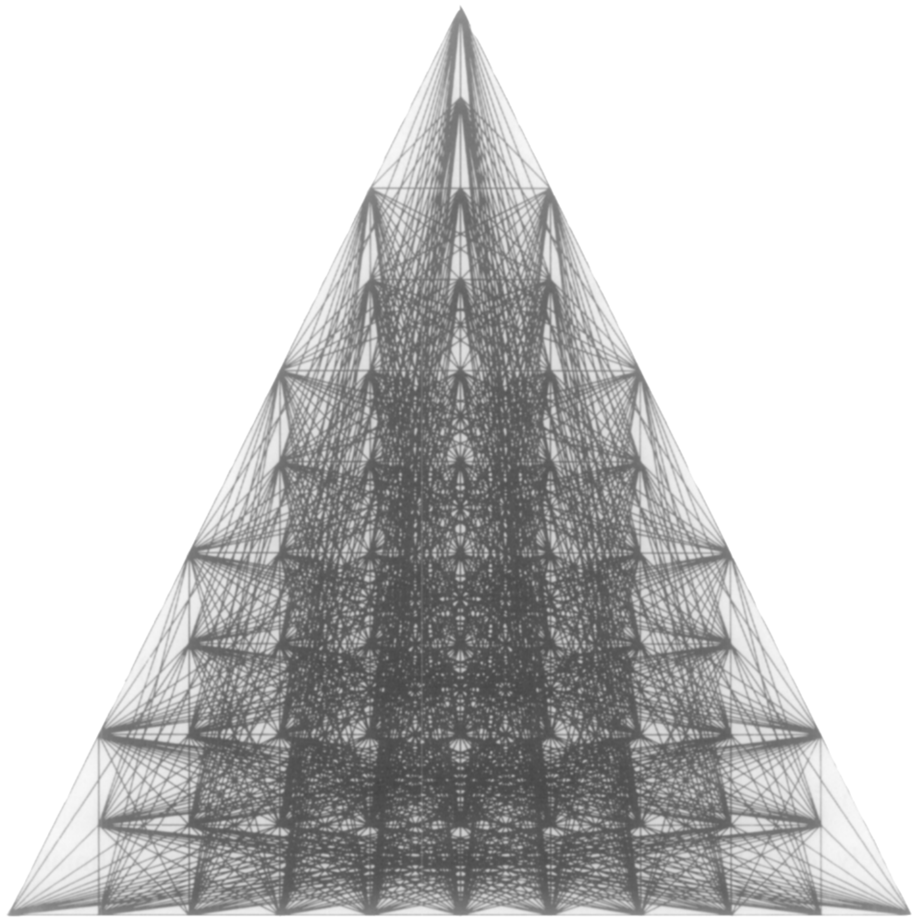

Fig. 11. Structural universe with 720 members for the problem in Fig. 10.

iterative COC solution with a prescribed minimum cross-sectional area of $z_a = 10^{-12}$ and a convergence tolerance value of $\bar{E} = 10^{-14}$ gave after 268 iterations $\Phi = 25.000000001168$.

5. Layout problems with alternate loading conditions

5.1. Plastic design

If the structure is subjected to several alternative loading conditions $(\boldsymbol{p}_1, \boldsymbol{p}_2, \ldots, \boldsymbol{p}_j, \ldots, \boldsymbol{p}_n)$ equilibrating the statically admissible stress fields $\boldsymbol{Q}_j$ $(1, 2, \ldots, n)$, our optimization problem in plastic design becomes

$$\min_{\boldsymbol{Q}_j^{\mathrm{S}}} \Phi = \int_D \bar{\psi} \, \mathrm{d}\boldsymbol{x} \,,$$

subject to

$$(\text{for all } \boldsymbol{x} \in D) \quad \bar{\psi}(\boldsymbol{x}) = \max_j \psi[\boldsymbol{Q}_j^{\mathrm{S}}(\boldsymbol{x})] \,, \tag{30}$$

where ψ is the specific cost requirement for a given stress vector $\boldsymbol{Q}_j^{\mathrm{S}}$ and $\bar{\psi}$ is the value of the specific cost (e.g., cross-sectional area) to be adopted in the optimal design.

For the above problem, the optimality criteria are ([2, (1.24) on p. 47])

$$\begin{aligned} &(\text{for all } \boldsymbol{x} \in D) \quad \boldsymbol{q}_j^K = \lambda_j(\boldsymbol{x}) \mathscr{G}\{\psi[\boldsymbol{Q}_j^{\mathrm{S}}(\boldsymbol{x})]\} \,, \\ &\lambda_j \geq 0 \,, \quad \lambda_j > 0 \quad \text{only if } \bar{\psi} = \psi(\boldsymbol{Q}_j^{\mathrm{S}}) \,, \quad \sum_j \lambda_j = 1 \,. \end{aligned} \tag{31}$$

Considering now the class of problems with a specific cost function $\psi = k|Q_j|$ where Q_j is a single-component generalized stress, and *two* loading conditions, the optimality criteria become

$$(\text{for } k|Q_1| = \bar{\psi} \,, \quad k|Q_2| < \bar{\psi} \,, \quad |Q_1| > 0) \quad q_1 = k \operatorname{sgn} Q_1 \,, \quad q_2 = 0 \,, \tag{32}$$

$$(\text{for } k|Q_2| = \bar{\psi} \,, \quad k|Q_1| < \bar{\psi} \,, \quad |Q_2| > 0) \quad q_2 = k \operatorname{sgn} Q_2 \,, \quad q_1 = 0 \,, \tag{33}$$

$$(\text{for } k|Q_1| = k|Q_2| = \bar{\psi} > 0) \,, \quad q_1 = \lambda k \operatorname{sgn} Q_1 \,, \quad q_2 = (1 - \lambda) k \operatorname{sgn} Q_2 \,, \quad 1 \geq \lambda \geq 0 \,, \tag{34}$$

$$(\text{for } Q_1 = Q_2 = \bar{\psi} = 0) \quad |q_1| + |q_2| \leq k \,. \tag{35}$$

It is relatively difficult to find a solution satisfying the above optimality conditions. However, it was shown independently by Nagtegaal and Prager [16], Spillers and Lev [17] and Hemp [15] that one can employ a superposition principle consisting of the following steps. First, construct the component load systems

$$p_1^* = \tfrac{1}{2}(p_1 + p_2)\,, \qquad p_2^* = \tfrac{1}{2}(p_1 - p_2)\,. \tag{36}$$

Then optimize the structure for p_1^* and p_2^* separately and add the corresponding specific costs ψ_1^* and ψ_2^*,

$$\psi = \psi_1^* + \psi_2^*\,. \tag{37}$$

The above specific cost (ψ) values represent the optimal solution for the two alternate loading conditions (p_1 and p_2). Denoting the adjoint strains of the optimal solutions for the component loads by $\bar{q}_1^*$ and $\bar{q}_2^*$, the adjoint strains for the original two loading conditions, satisfying (32)–(35), are given by

$$\bar{q}_1 = \bar{q}_1^* + \bar{q}_2^*\,, \qquad \bar{q}_2 = \bar{q}_1^* - \bar{q}_2^*\,. \tag{38}$$

The above superposition principle will be illustrated with a simple example. Determine the optimal truss layout for the two load conditions in Figs. 12(a,b). The component loads and the corresponding optimal solutions are given in Figs. 12(c,d), in which the adjoint displacements, respectively, are (with $k = 1$)

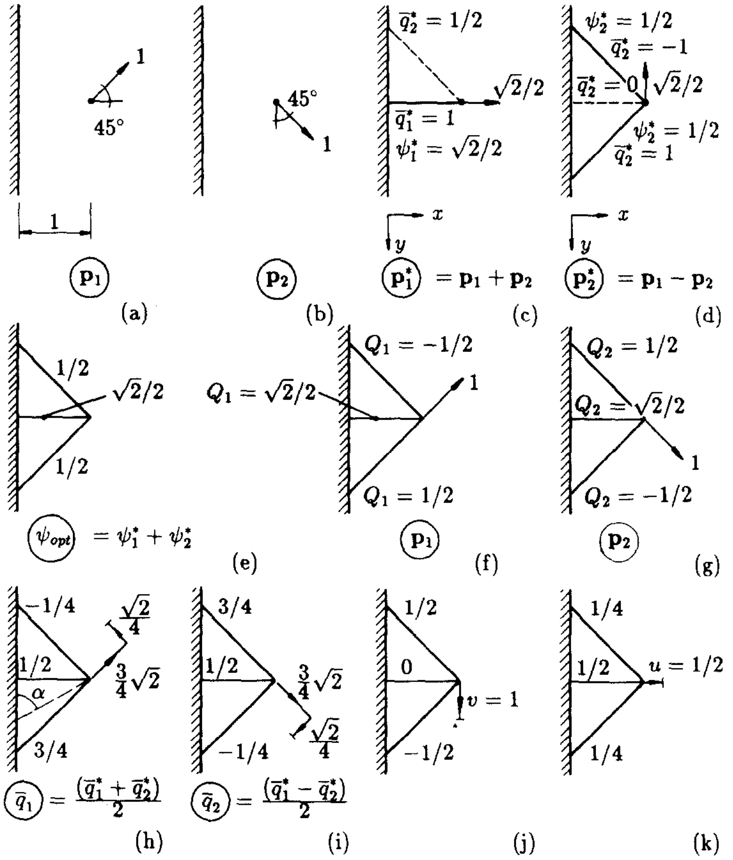

Fig. 12. Optimal layout for plastic design: two alternate loads.

$$\bar{u}_1^* = x\,, \qquad \bar{v}_1^* \equiv 0\,; \qquad \bar{u}_2^* = 0\,, \qquad \bar{v}_2^* = 2x\,, \tag{39}$$

where $\bar{u}$ and $\bar{v}$ denote displacements in the x and y directions. It can be readily checked that the displacements in (39) give the strains in Figs. 12(c,d) and that the latter satisfy the optimality conditions in (21) and (22) (Section 2.3.2). The superimposed optimal solution for the two alternate loads is shown in Fig. 12(e) and the member forces for the two load conditions in Figs. 12(f,g). Note that only *statical* admissibility is required in plastic design. It can be seen from the above figures that all members are fully stressed ($k|Q_j| = \bar{\psi}$ with $k = 1$) for *both* loading conditions and hence optimality criterion (34) applies. The adjoint strains for the alternate loads are given in Figs. 12(h,i), calculated on the basis of (38). Kinematic admissibility of the strains in Fig. 12(i), for example, can be checked by superimposing the simple displacement fields in Figs. 12(j,k). The strain fields in Figs. 12(h,i) satisfy the optimality criterion (34) with $\lambda = 1/4$, $\lambda = 1/2$ and $\lambda = 3/4$ for the top, middle and bottom members, respectively, and hence optimality of the considered solution is confirmed.

For layout optimality, it is still necessary to show that the strains for nonoptimal directions also satisfy conditions (35). For an arbitrary angle α, the strains become (Fig. 12(h))

$$\begin{aligned} \varepsilon_1 &= \tfrac{1}{4}\sqrt{2}\sin\alpha[3\cos(135° - \alpha) - \cos(45° - \alpha)]\,, \\ \varepsilon_2 &= \tfrac{1}{4}\sqrt{2}\sin\alpha[\cos(135° - \alpha) + 3\cos(45° - \alpha)]\,. \end{aligned} \tag{40}$$

By condition (35),

$$|\varepsilon_1| + |\varepsilon_2| \leq k\,, \tag{41}$$

for any value of α in an optimal solution. Indeed, relations (40) and (41) with $k = 1$ imply

$$\tfrac{1}{4}\sin\alpha[|3(\sin\alpha - \cos\alpha) - (\sin\alpha + \cos\alpha)| + |3(\sin\alpha + \cos\alpha) - (\sin\alpha - \cos\alpha)|] \leq 1\,, \tag{42}$$

which can readily be shown to be correct. The actual variation of the left-hand side of relation (42) is given in Fig. 13. It can be seen that $|\varepsilon_1| + |\varepsilon_2|$ only takes on the value k in the optimal

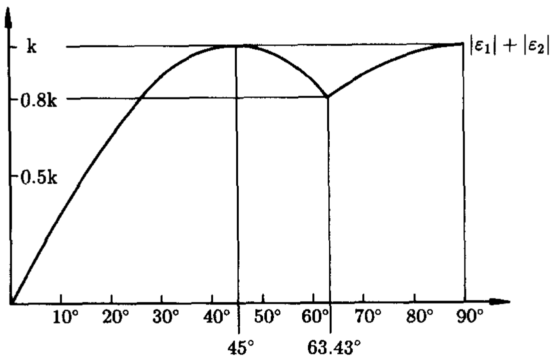

Fig. 13. Check on optimality condition (35).

directions and condition (41) is also satisfied for all other directions. The above problem was investigated in an earlier publication [18].

The superposition principle discussed here has been extended to an arbitrary number (2^n) of loading conditions by Rozvany and Hill [19].

5.2. Elastic design for compliance

For several loading conditions ($k = 1, 2, \ldots, s$) and several displacement conditions ($j = 1, 2, \ldots, v$), the optimality condition in Fig. 5 of Part I [1] changes to

$$\bar{q}_k^K = \sum_j \nu_{jk}[F]\bar{Q}_j^S , \tag{43}$$

$$\mathscr{G}_{,z}[\psi(z)] + \sum_j \sum_k \nu_{jk}\bar{Q}_j^{S,K} \cdot \{\mathscr{G}[F]\}Q_k^{S,K} = 0 . \tag{44}$$

Considering the class of simple problems with $\psi = cz$, $[F] = 1/rz$, and two compliance constraints [with scalar stresses $\bar{Q}_j \to Q_k$ in (43)] $\int_D (Q_k^2/rz)\,dx = C_k$ ($k = 1, 2$), (43) and (44) reduce to

$$\bar{q}_k = \nu_{kk}Q_k/rz , \quad k = 1, 2 , \tag{45}$$

$$c - \sum_{k=1}^{2} \nu_{kk}Q_k^2/rz = 0 \;\Rightarrow\; z = \sqrt{(\nu_{11}Q_1^2 + \nu_{22}\dot{Q}_2^2)/rc} . \tag{46}$$

The above optimality criterion is difficult to handle in analytical derivations, but is highly suitable for an iterative COC procedure.

For a discretized formulation, the values of the Lagrangians ν_{11} and ν_{22} can be calculated from the compliance constraints [cf. (33) in Section 3.6 of Part I]:

$$C_k = \sum_A \frac{Q_{ik}^2\delta_i}{r\sqrt{(\nu_{11}Q_{i1}^2 + \nu_{22}Q_{i2}^2)/rc}} + \sum_P \frac{Q_{ik}^2\delta_i}{rz_a} , \quad k = 1, 2 , \tag{47}$$

where δ_i is the element length. Equations (47) can, in general, only be solved iteratively.

In the case of a symmetric boundary and two anti-symmetric load systems (as in Fig. 12), we have $\nu_{11} = \nu_{22} = \nu$. Moreover, we can carry out the analysis for one load condition only and denote by Q and $\hat{Q}$ the stresses in the corresponding elements of the two symmetric half-structures. Then (46) reduces to

$$z = \sqrt{\nu(Q^2 + \hat{Q}^2)/rc} . \tag{48}$$

If the entire structure has $2n$ elements and they are numbered in the same symmetric sequence for the two halves, then the discretized equivalent of (48) becomes

$$z_i = z_{i+n} = \sqrt{\nu(Q_i^2 + Q_{i+n}^2)/rc} , \quad i = 1, 2, \ldots, n . \tag{49}$$

Moreover, for the considered symmetric problems with $C_1 = C_2$, (47) reduces to

$$\sqrt{\nu} = \sum_A \frac{Q_i^2 \delta}{\sqrt{r(Q_i^2 + Q_{i\pm n}^2)/c}} \Big/ \left(C - \sum_P \frac{Q_i^2 \delta}{r z_a}\right), \tag{50}$$

where in the subscript '±', we have '+' for $1 \leq i \leq n$ and '−' for $n+1 \leq i \leq 2n$.

The problem in Fig. 12(a,b) was solved for an elastic compliance constraint using the above iterative COC procedure with 7170 potential bars. After 1500 iterations a total weight value of $\Phi = 3.49295726$ was obtained. The plot of bars having a cross-sectional area over $z = 0.08$ is shown in Fig. 14 (continuous lines), in which three different line thicknesses show various ranges of member sizes (z). The 'structural universe' consisted of 11×21 grid-points and the connecting members were restricted to slopes of 0, 1:1, 1:2, . . . , 1:10, 2:3, 2:5, . . . , 2:9 and their reciprocals (see part of the structural universe in the top right corner of Fig. 14). The exact analytical solution for the above problem is, as yet, not known to the authors. However, if we assume a symmetric two-bar system (broken lines in Fig. 14), then the optimal solution within this topology can be determined easily. It can be shown from statical considerations that for $p_1 = 1$ the member forces are

$$N_1 = \frac{1}{2\sqrt{2}}\left(\frac{1}{\cos\alpha} + \frac{1}{\sin\alpha}\right), \qquad N_2 = \frac{1}{2\sqrt{2}}\left(\frac{1}{\cos\alpha} - \frac{1}{\sin\alpha}\right), \tag{51}$$

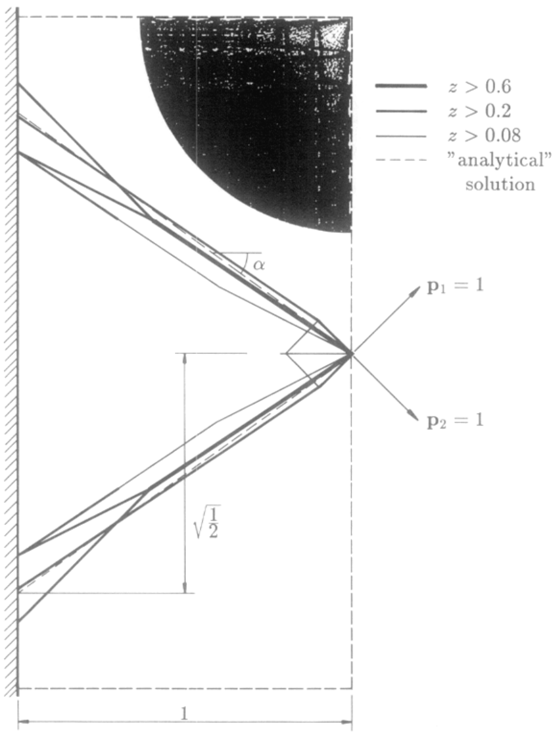

Fig. 14. Iterative COC solution for a compliance constraint with two alternate loading conditions and part of the structural universe.

and due to symmetry of the solution we have

$$C = 1 = \frac{N_1^2}{A} L + \frac{N_2^2}{A} L = \frac{1}{A \cos \alpha \sin^2(2\alpha)}, \tag{52}$$

where A is the cross-sectional area and L is the member length. The relation (52) implies

$$A = \frac{1}{\cos \alpha \sin^2(2\alpha)}, \qquad \Phi = 2AL = \frac{2}{\cos^2 \alpha \sin^2(2\alpha)}. \tag{53}$$

Then the usual stationarity condition ($\mathrm{d}\Phi / \mathrm{d}\alpha = 0$) implies

$$2 \cos \alpha \sin \alpha \sin^2(2\alpha) - 4 \cos^2 \alpha \sin(2\alpha) \cos(2\alpha) = 0, \qquad \tan^2 \alpha = 1/2,$$

$$\Phi = 27/8 = 3.375, \qquad A = 27/16\sqrt{1.5} = 1.37783798, \qquad \alpha = 35.26438968^\circ. \tag{54}$$

The optimal two-bar system, having a slope of $\tan \alpha = 1/\sqrt{2}$ is shown in broken line in Fig. 14. Since this system has 3.495% lower weight than the COC solution with 7170 potential members, it could be the absolute optimal layout. It can be seen from Fig. 14 that the COC procedure, within the limited range of admissible member slopes, is trying to achieve this solution.

Quite recently, another iterative COC calculation with 12202 members (an 11×21 grid as before, but with all possible connecting members within each half-grid) gave a weight of 3.375668 which is only 0.0198% above the assumed analytical solution. This numerical solution consisted of two heavy bars in the vicinity of the broken lines in Fig. 14, which confirms the assumed analytical solution.

NOTE. It can be seen from Sections 5.1 and 5.2 that unlike for a single load condition, the solutions for plastic design and elastic compliance design differ significantly if several alternate loads are considered.

The authors were informed recently that in an unpublished symposium paper Bendsøe and Ben-Tal [29], who used a different method, also presented optimal truss layouts involving several thousand potential members.

6. Generalized shape optimization

Before discussing the implications of layout optimization in shape optimization, we show one more iterative COC result concerning a simply supported truss with a central point load (Figs. 15(a–d), which show one half of the truss for various ranges of cross-sectional areas). For a comparison, Figs. 15(e–i) show COC solutions for a plate of variable thickness (t) with the same support and load conditions.

It was mentioned in the Introduction that in generalized shape optimization one type of region, termed perforated (grey) region, contains a fine system of cavities or, theoretically, an infinite number of internal boundaries. A similar result was obtained in plate optimization

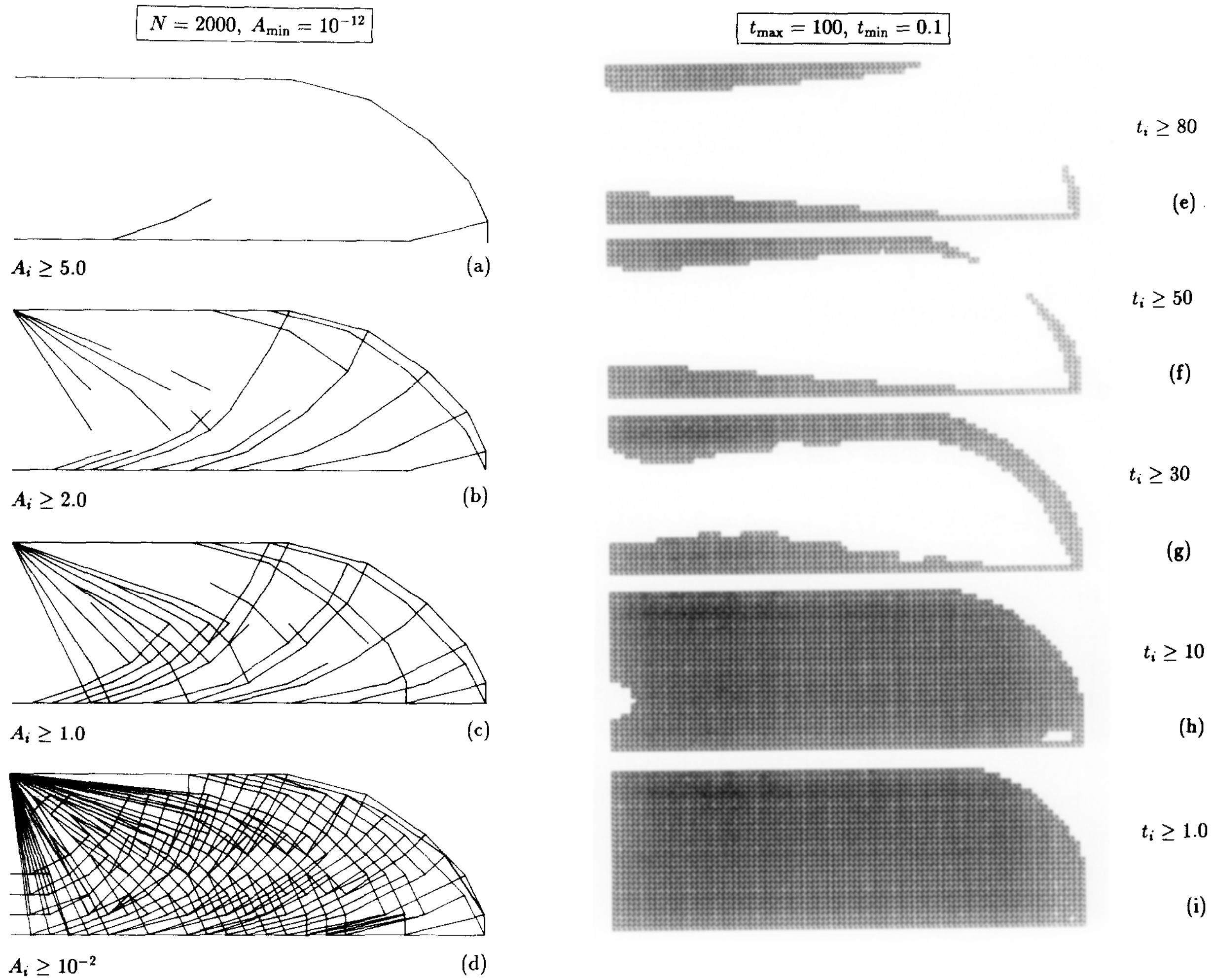

Fig. 15. A comparison of a truss layout and a plate of variable thickness obtained by the COC method.

where optimal solid and perforated plates were found ([27, 28], see also [21, 22]) to contain systems of ribs of infinitesimal spacing and hence the thickness function has an infinite number of discontinuities over a finite width. Although the material in these problems is isotropic, the 'homogenization' method consists of replacing ribbed or fibrous elements with homogeneous but anisotropic elements whose stiffness or strength is direction- but not location-dependent within the element (e.g. [28]).

From a historical point of view, the basic idea of homogenization was introduced already by Prager and the second author (e.g. [8, 9]), although they used the terms 'grillage-like continua' and 'truss-like continua'. In these structures, a theoretically infinite number of bars or beams occur over a unit width but the above authors replaced this system with a continuum, whose specific cost, stiffness and strength depended on the 'lumped' width of the bars or beams over a unit width. This concept was clearly equivalent to homogenization, but in an engineering rather than a mathematical context. Applications of homogenization in generalized shape optimization were discussed in pioneering contributions by Bendsøe (e.g.

[23]) which represent one of the most important recent developments in structural optimization.

Returning now to the shape optimization of a perforated plate in bending or in plane stress, various mathematical studies suggested that the optimal microstructure consists of ribs of first- and second-order infinitesimal width in the two principal directions, if the structure is optimized for a given compliance. The stiffness and cost properties of this microstructure were discussed in papers by Rozvany et al. [22]. For a zero value of Poisson's ratio, for example, the non-dimensionalized specific cost becomes

$$\psi = (S_1 - 2S_1S_2 + S_2)/(1 - S_1S_2)\,, \tag{55}$$

where S_1 and S_2 are the non-dimensionalized stiffnesses in the principal directions. The above formula, for example, gives $\psi = 1$ for $S_1 = S_2 = 1$ (solid or 'black' regions) and $\psi = 0$ for $S_1 = S_2 = 0$ (empty or 'white' regions). On the basis of the specific cost function in (55), analytical solutions were obtained for axisymmetric perforated plates [22]. Naturally, the same cost functions could be used for numerical shape optimization, and should give the correct solution for plates in plane stress or bending. This development is pursued currently by the authors.

The main aim of the investigations by Bendsøe [23] and Kikuchi et al. [24] is to come up with a practical topology, in which the perforated ('grey') areas disappear and the optimal structure consists of solid ('black') and empty ('white') regions only. This procedure can be seen from Fig. 16(a,b), in which Olhoff et al. [26] first determined the approximate optimal topology (Fig. 16(a)) for the support condition and loading considered in Fig. 15, and then carried out a separate shape optimization (Fig. 16(b)) for the more detailed design conditions. This 'homogenization' method, indeed, gives negligibly small perforated (grey) areas, as can be observed in Fig. 16(a), and also in Fig. 17 which was obtained by Kikuchi et al. [24] for the load and support conditions in Fig. 9. The latter seems to give the same topology, irrespective of the number of elements (N) employed.

The following circumstantial evidence seems to indicate that the *exact* optimal topologies differ from those obtained by the homogenization method (e.g. Figs. 16(b) and 17):

- In the analytical solutions obtained for perforated plates [22], a high proportion of the plate area is covered by perforated (grey) areas.
- It was shown previously [22] that the solution for very low volume fractions tends to that for grid-type structures (Michell frames or least-weight grillages). This was also observed by Prager who commented on some optimal solid plate designs by Cheng and Olhoff [27]. It was also noted [22] that, as the volume fraction increased progressively in analytical solutions, solid (black) regions developed in areas where the ribs in the perforated regions had the greatest density. Making use of this observation, the grid-type solutions in Figs. 15(a–d) imply the topology in Fig. 16(c) (graphics by Dr. Gollub), in which the width of the solid regions is based on the cross-sectional areas of the 'concentrated' bars along the top and bottom chords of the truss. The spacing of the members in the perforated region is theoretically infinitesimal, but a finite number of members would have to be used in any practical solution. In the neighbourhood of the top right corner, we have an empty (white) region. It can also be observed that the 'homogenized' solution in Fig. 16(a) tries to achieve the solution in Fig. 16(c), except that in areas of low rib density (e.g. right bottom region

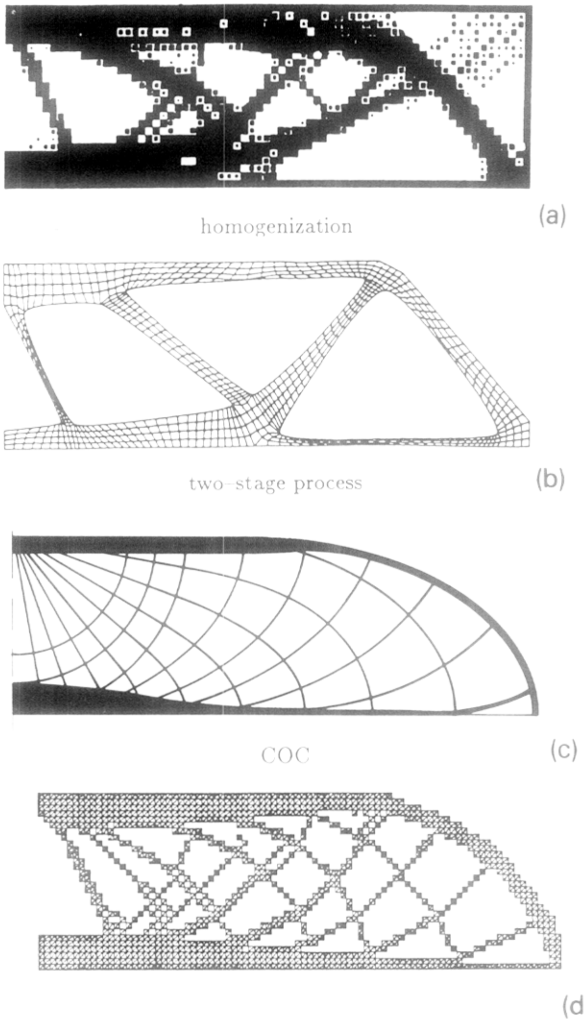

Fig. 16. (a), (b) Simplified topology derived by Olhoff and Rasmussen for the problem treated in Fig. 4. (c) The exact topology suggested by COC layout solutions in Fig. 15. (d) Solution obtained by a modified homogenization method (see Section 6.1).

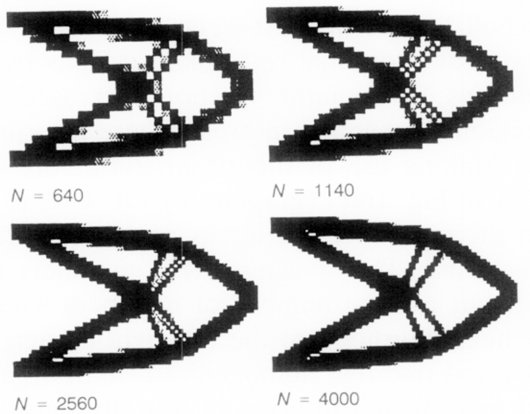

Fig. 17. Simplified topology obtained by Kikuchi for the problem treated in Fig. 6 [24].

inside the chord) it comes up with empty regions. As Bendsøe pointed out at a recent meeting, this can be attributed to the fact that here non-optimal microstructures were used for the perforated (grey) regions. Whilst this does not change the cost of solid (black) and empty (white) regions, it does increase artificially the cost of perforated (grey) regions and hence it tends to suppress the latter.

- The solutions for plates of varying thickness represent an 'isotropized' version of the exact solution. This can be observed by comparing Figs. 15(e–i) with Fig. 16(c). The plate thickness in the former is roughly proportional to the average material density over the latter, with ribs occurring in Figs. 15(e–i) along the solid regions of Fig. 16(c). This is a further confirmation of the improved topology in Fig. 16(c). Moreover, a modified isotropized homogenization method (Section 6.1) fully confirmed the solution in Fig. 16(c), as can be seen from Fig. 16(d).

REMARK. The contention that existing homogenization methods give a simplified topology compared to the exact solution by no means represents a criticism of these extremely important techniques. Such 'condensed' topologies are in fact very practical because, naturally, it is impossible to use an infinitesimal bar spacing in real structures. However, the exact

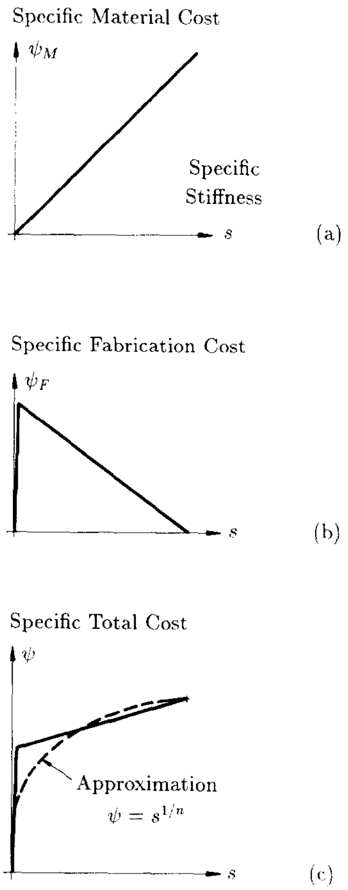

Fig. 18. Suppression of 'grey' regions in isotropized solutions.

optimal topology can also be of practical significance, because the client could be told by the designer that further weight savings can always be achieved by increasing the number of 'holes' in the design and then the former could decide as to how far he can go within realistic manufacturing capabilities.

6.1. An alternative method for suppressing perforated (grey) regions

Since the use of non-optimal microstructures homogenized into an anisotropic continuum introduces some unknown penalty for 'grey' regions into shape optimization, the perforated (grey) regions could also be suppressed by using an isotropic microstructure but with a suitable penalty function for such regions. This can also be justified on practical grounds, as can be seen from the argument that follows.

As a first approximation, we could assume that the specific material cost (i.e. weight) is roughly proportional to the specific stiffness of perforated regions (Fig. 18(a), which is also valid for plates of variable thickness). On the other hand, the extra manufacturing cost of cavities would increase with the size of the cavities if we consider a casting process requiring some sort of formwork for the cavities (Fig. 18(b)). Note that for empty (white) macroscopic regions with $s = 0$ the manufacturing cost also becomes zero. The specific total cost and its suitable approximation is shown in Fig. 18(c). The use of the above type of cost function promotes the suppression of perforated (grey) areas in isotropized designs which require only one design parameter (s) per element. The introduction of orthogonal cavities in the usual homogenization process [23, 24] requires 3 design variables per element for two-dimensional systems and 6 variables for three-dimensional ones. The solution in Fig. 16(d) was obtained with an n-value of 1.86 in Fig. 18(c), and represents a topology closer to the 'exact' optimal design than the design in Fig. 16(b). As expected, simpler topologies can be obtained by adopting a higher n-value (i.e. by increasing the penalty for grey regions).

7. Conclusions

- The iterative COC method enables us, probably for the first time in the history of structural optimization
  (a) to optimize simultaneously the topology and geometry of grid-type structures (trusses, grillages, shell-grids, etc.),
  (b) for a compliance constraint (with future extensions to any combination of the usual design conditions such as stress, displacement, natural frequency, stability, etc. constraints),
  (c) using a fully automatic method capable of handling many thousand potential members.
- Shape optimization by 'homogenization' is essentially a numerical approximation of exact solutions in which perforated (grey) regions tend to be suppressed. The discretization errors in topologies obtained by this method can be assessed by a comparison with COC solutions for grid-like systems (e.g. Figs. 15(a–d)) or for 'isotropized' systems (e.g. Figs. 15(e–i)). With a suitable penalty formulation, the latter could also be used for suppressing perforated (grey) regions in shape optimization.

References

[1] G.I.N. Rozvany and M. Zhou, The COC algorithm, Part I: Cross-section optimization or sizing, Comput. Methods Appl. Mech. Engrg. 89 (1991) 281–308.
[2] G.I.N. Rozvany, Structural Design via Optimality Criteria (Kluwer Acad. Publ., Dordrecht, 1989).
[3] A.G.M. Michell, The limits of economy of material in frame-structures, Phil. Mag. 8 (47) (1904) 589–597.
[4] J.C. Maxwell, On reciprocal figures, frames and diagrams of force, Trans. Roy. Soc. Edinb. 26 (1); also in: W.D. Niven, ed., Scientific Papers 2 (Univ. Press, Cambridge, 1872) 174–177.
[5] U. Kirsch, On the relationship between structural topologies and geometries, Struct. Optim. 2 (1989) 39–45.
[6] W. Prager, Introduction to Structural Optimization, CISM 212 (Springer, Vienna, 1974).
[7] G.I.N. Rozvany, Optimal Design of Flexural Systems (Pergamon, Oxford, 1976); Russian translation (Stroiizdat, Moscow, 1980).
[8] W. Prager and G.I.N. Rozvany, Optimization of structural geometry, in: A.R. Bednarek and L. Cesari, eds., Dynamical Systems (Academic Press, New York, 1977) 265–293.
[9] G.I.N. Rozvany, Optimality criteria for grids, shells and arches, in: E.J. Haug and J. Cea, eds., Optimization of Distributed Parameter Structures, Proc. NATO ASI held in Iowa City (Sijthoff & Noordhoff, Alphen aan den Rijn, Netherlands, 1981) 112–151.
[10] G.I.N. Rozvany and T.G. Ong, Minimum-weight plate design via Prager's layout theory (Prager Memorial Lecture), in: Mota Soares, ed., Computer Aided Optimal Design: Structural and Mechanical Systems, Proc. NATO ASI held in Troia, Portugal, 1986 (Springer, Berlin, 1987) 165–179.
[11] G.I.N. Rozvany, W. Gollub and M. Zhou, Layout optimization in structural design, in: B.H.V. Topping, ed., Proc. NATO ASI, Optimization and Decision Support Systems in Civil Engineering, 25 June–7 July 1989, Edinburgh (Kluwer, Dordrecht, 1990).
[12] G.I.N. Rozvany, Structural layout theory: The present state of knowledge, in: E. Atrek, R.H. Gallagher, M.K. Ragsdell and O.C. Zienkiewicz, New Directions in Optimum Structural Design (Wiley, Chichester, England, 1984) 167–195.
[13] G.A. Hegemier and W. Prager, On Michell trusses, Internat. J. Mech. Sci. 11 (1969) 209–215.
[14] G.I.N. Rozvany and W. Gollub, Michell layouts for various combinations of line supports, Part I, Internat. J. Mech. Sci., in press.
[15] W.S. Hemp, Optimum Structures (Clarendon, Oxford, 1973).
[16] J.C. Nagetegaal and W. Prager, Optimal layout of a truss for alternative loads, Internat. J. Mech. Sci. 15 (7) (1973) 583–592.
[17] W.R. Spillers and O. Lev, Design for two loading conditions, Internat. J. Solids and Structures 7 (1971) 1261–1267.
[18] G.I.N. Rozvany, Analytical treatment of some extended problems in structural optimization, Part II, J. Struct. Mech. 3 (4) (1974) 387–402.
[19] G.I.N. Rozvany and R.D. Hill, Optimal plastic design: Superposition principles and bounds on the minimum cost, Comput. Methods Appl. Mech. Engrg. 13 (2) (1978) 151–173.
[20] G.I.N. Rozvany, W. Gollub and M. Zhou, Michell layouts for various combinations of lines supports, Part II, Internat. J. Mech. Sci. (1991) submitted.
[21] G.I.N. Rozvany, N. Olhoff, J.-T. Cheng and J.E. Taylor, On the solid plate paradox in structural optimization, J. Struct. Mech. 10 (1) (1982) 1–32.
[22] G.I.N. Rozvany, N. Olhoff, M.P. Bendsøe, T.G. Ong, R. Sandler and W. T. Szeto, Least-weight design of perforated elastic plates, I and II. Internat. J. Solids and Structures 23 (4) (1987) 521–536, 537–550.
[23] M.P. Bendsøe, Optimal shape design as a material distribution problem, Struct. Optim. 1 (4) (1989) 193–202.
[24] N. Kikuchi and K. Suzuki, Shape and topology optimization by the homogenization method, in: G.I.N. Rozvany, ed., Proc. CISM Advanced School, Shape and Layout Optimization of Structural Systems (Udine, July 1990) (Springer, Vienna, 1991).
[25] T.G. Ong, G.I.N. Rozvany and W.T. Szeto, Least-weight design of perforated elastic plates for given compliance: Nonzero Poisson's ratio, Comput. Methods Appl. Mech. Eng. 66 (3) (1988) 301–322.
[26] N. Olhoff, M.P. Bendsøe and J. Rasmussen, On CAD-integrated structural topology and design optimization, Comput. Methods Applied Mech. Engrg. 89 (1991) 259–279.

[27] K.-T. Cheng and N. Olhoff, An investigation concerning optimal design of solid elastic plates, Internat. J. Solids and Structures 17 (3) (1981) 305–323.
[28] N. Olhoff, K.A. Lurie, A.V. Cherkaev and A.V. Fedorov, Sliding regimes and anisotropy in optimal design of vibrating axisymmetric plates, Internat. J. Solids and Structures 17 (1981) 931–948.
[29] M.P. Bendsøe and A. Ben-Tal, Truss topology optimization, Symp. Polish Acad. Sci. Optimal Design and Control of Structures, Jablonna, Poland, June 1990.